of the charge-transfer excitation and in the reduction potential for this series of cobalt(III) chelates. The proximity of the $^1T_{2g}$ and CT excited states explains why the $^1T_{2g} \leftarrow {}^1A_{1g}$ transition is difficult to observe.

Registry No. *fac*-**1**, 60733-43-9; *mer*-**1**, 60684-52-8; *fac*-**2**, 41765-60-0; *mer*-**2**, 41768-47-2; *fac*-**3**, 105617-40-1; *mer*-**3**, 105617-42-3; **4**, 21679-46-9; *fac*-**5**, 41768-44-9; *mer*-**5**, 41768-43-8; *fac*-**6**, 23331-43-3; *mer*-**6**, 23302-00-3; *fac*-**7**, 41768-44-9; *mer*-**7**, 41768-43-8; **8**, 21679-34-5; **9**, 31125-84-5; *fac*-**10**, 105617-45-6; *mer*-**10**, 105617-41-2; **11**, 16702-37-7; **12**, 14877-41-9; **13**, 15169-25-2; **14**, 16702-37-7; *fac*-**15**, 105563-50-6; *mer*-**15**, 105617-43-4; *fac*-**16**, 105563-51-7; *mer*-**16**, 105617-44-5.

Contribution from the Department of Chemistry,
McGill University, Montreal, Quebec, Canada H3A 2K6

Spin-Lattice Relaxation Time Studies and Vibrational Spectra of Solid Tricarbonyl(η^7-tropylium)chromium(0) and -molybdenum(0) Tetrafluoroborates, $[(\eta^7\text{-}C_7H_7)M(CO)_3]BF_4$ (M = Cr, Mo)

Pierre D. Harvey, Ian S. Butler,* and Denis F. R. Gilson*

Received April 25, 1986

The proton and ^{19}F spin-spin lattice relaxation times (T_1) of the solid, group VIB (6^{46}) tricarbonyl(η^7-tropylium)metal(0) tetrafluoroborates, $[(\eta^7\text{-}C_7H_7)M(CO)_3]BF_4$ (M = Cr, Mo), have been measured over the 296-93 K temperature range. The activation energies (kJ mol^{-1}) for arene ring rotation in the two complexes are quite similar: Cr, 12.8; Mo, 13.6. X-ray powder diffraction patterns of the Cr, Mo, and W complexes at room temperature indicate that the three complexes are isostructural. The activation energies (kJ mol^{-1}) for BF_4^- reorientation are different: Cr, 6.77; Mo, 12.3. Nonbonded atom-atom potential calculations show that the barriers to tropylium ring rotations are due to ring-carbonyl and ring-BF_4^- interactions in about equal amounts. Similar calculations on BF_4^- reorientation indicate that rotations around the 3-fold axes have lower barriers than do rotations about the 2-fold axes. The FT-IR and Raman spectra of the Cr and Mo complexes have also been investigated at room and low temperature, and some vibrational assignments are proposed. The spectroscopic results, together with differential scanning calorimetry data, confirm the absence of any phase changes for the complexes in the 296-80 K temperature range.

Introduction

The possible bonding modes and conformations of the aromatic rings in π-arene organometallic complexes of the type $(\eta^n\text{-}C_nH_n)M(CO)_3$ (M = transition metal; n = 4-7) have been the subject to renewed interest of late.[1-3] It is now clear that the arene rings do not possess the ideal symmetries expected for a regular square, pentagon, hexagon, etc.[4-15] In addition, very low barriers to ring rotation are predicted for $(\eta^4\text{-}C_4H_4)$-, $(\eta^5\text{-}C_5H_5)$- and $(\eta^7\text{-}C_7H_7)ML_3$ complexes.[3] For a clearer understanding of the motional behavior of the π-arene compounds, it is important to have information on the dynamics, as well as the structures of the complexes, in order to obtain realistic estimates of the potential barriers to arene group rotation in the solids.

Over the past 5 years, there have been several investigations of the barriers to π-arene ring rotation in solid organometallic complexes, e.g. the cyclobutadienyl ring in $(\eta^4\text{-}C_4H_4)Fe(CO)_3$[16] and the cyclopentadienyl ring in various derivatives such as $(\eta^5\text{-}C_5H_5)Mn(CO)_3$.[17-19] The principal approaches have been to study the temperature dependence of the proton spin-lattice relaxation times and to perform nonbonded atom-atom potential calculations. The calculations have provided useful information on the origin and magnitude of the various contributions to the rotational barriers,[19,20] which are directly dependent on the packing and the sites occupied by the molecules in the unit cell. Chhor and Lucazeau[21-23] have used vibrational spectroscopy and neutron-scattering techniques to estimate the barrier heights to ring rotation in several solid organometallic systems.

A natural extension of the earlier work on π-arene ring systems in organometallic complexes would be to the 7-membered tropylium ring (C_7H_7) in such complexes as $TrV(CO)_3$ and $[TrM(CO)_3]BF_4$ (Tr = $\eta^7\text{-}C_7H_7$; M = Cr, Mo, W). The vanadium complex is not suitable for NMR studies because of its paramagnetism.[24] The crystal structure of the molybdenum salt has been published, and it appears that it was difficult to locate the

(1) Chinn, J. W., Jr.; Hall, M. B. *J. Am. Chem. Soc.* **1983**, *105*, 4930.
(2) Chinn, J. W., Jr.; Hall, M. B. *Inorg. Chem.* **1983**, *22*, 2759.
(3) Albright, T. A. *Acc. Chem. Res.* **1982**, *15*, 149.
(4) Day, V. W.; Reimer, K. J.; Shaver, A. *J. Chem. Soc., Chem. Commun.* **1975**, 404.
(5) Mitschler, A.; Rees, B.; Lehmann, M. S. *J. Am. Chem. Soc.* **1978**, *100*, 3390.
(6) Day, V. W.; Stults, B. R.; Reimer, K. J.; Shaver, A. *J. Am. Chem. Soc.* **1974**, *96*, 1227.
(7) Byers, L. R.; Dahl, L. F. *Inorg. Chem.* **1980**, *19*, 277 and references therein.
(8) Fitzpatrick, P. J.; Lepage, Y.; Sedman, J.; Butler, I. S. *Inorg. Chem.* **1981**, *20*, 2852.
(9) Fitzpatrick, P. J.; Lepage, Y.; Butler, I. S. *Acta Crystallogr., Sect. B: Struct. Crystallogr. Cryst. Chem.* **1981**, *37*, 1052.
(10) Yannoni, C. S.; Caeser, C. P.; Dailey, B. P. *J. Am. Chem. Soc.* **1967**, *89*, 2833.
(11) Bailey, D.; Buckingham, A. D.; Rest, A. J. *Mol. Phys.* **1973**, *26*, 233.
(12) Emsley, J. W.; Lindon, J. C. *Mol. Phys.* **1974**, *28*, 1373.
(13) Diehl, P.; Moia, F.; Boesiger, H.; Wirz, J. *J. Mol. Struct.* **1983**, *98*, 297.
(14) Gilson, D. F. R. *J. Mol. Struct.* **1985**, *127*, 121.
(15) Gilson, D. F. R.; Fitzpatrick, P. J.; Butler, I. S. *Organometallics* **1984**, *3*, 387.
(16) Harvey, P. D.; Butler, I. S.; Gilson, D. F. R. *Inorg. Chem.* **1986**, *25*, 1009.
(17) Butler, I. S.; Fitzpatrick, P. J.; Gilson, D. F. R.; Gomez, G.; Shaver, A. *Mol. Cryst. Liq. Cryst.* **1981**, *71*, 213.
(18) Gilson, D. F. R.; Gomez, G.; Butler, I. S.; Fitzpatrick, P. J. *Can. J. Chem.* **1983**, *61*, 737.
(19) Gilson, D. F. R.; Gomez, G. *J. Organomet. Chem.* **1982**, *124*, 41.
(20) Cambell, A. J.; Fyfe, C. A.; Harold-Smith, D.; Jeffrey, K. R. *Mol. Cryst. Liq. Cryst.* **1976**, *36*, 1.
(21) Chhor, K.; Lucazeau, G. *Inorg. Chem.* **1984**, *23*, 462.
(22) Lucazeau, G.; Chhor, K.; Pommier, C. *Spectrosc.: Int. J.* **1983**, *2*, 79.
(23) Chhor, K.; Lucazeau, G. *J. Raman Spectrosc.* **1982**, *13*, 235.
(24) Allegra, G.; Perego, G. *Ric. Sci., Parte 2: Ser. A* **1961**, *1*, 362.

0020-1669/87/1326-0032$01.50/0

F atoms in the BF_4^- ions because of dynamic disorder.[25] We present here the results of an investigation of the barriers to reorientation of the Tr ring and the BF_4^- ion in the solid tricarbonyl(η^7-tropylium)chromium(0) and -molybdenum(0) tetrafluoroborates, $[TrM(CO)_3]BF_4$, by both NMR T_1 measurements and vibrational spectroscopy. Nonbonded atom–atom potential calculations for the Mo complex and X-ray powder patterns for the Cr, Mo, and W complexes are also reported in this paper.

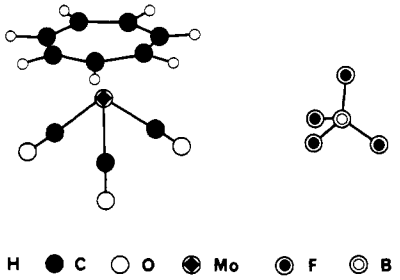

$[(\eta^7\text{-}C_7H_7)Mo(CO)_3]BF_4$

Experimental Section

The $[TrM(CO)_3]BF_4$ (M = Cr, Mo, W) salts were prepared by the literature procedure[26] and were purified by triple recrystallization from spectrograde acetone (Anachemia Co.). The samples were stored in sealed vials in vacuo or under a nitrogen atmosphere; when not in use, they were kept in the dark.

The X-ray powder diffraction patterns were measured at room temperature on a Debye-Scherrer camera (ϕ = 28.65 mm) using Cu K$\bar{\alpha}$ (1.541 78 Å) radiation and a nickel filter. The orange, polycrystalline samples were carefully ground up and the placed in 0.5-mm-diameter capillaries. The indexations were obtained by using a program written for the Université de Montréal computer.

Spin–lattice relaxation times were measured at 33 MHz by using a Spin-Lock CPS2 pulsed NMR spectrometer. A 180°–t–90° pulse sequence was used, and the free induction decays were captured on a Biomation 805 transient recorder and then plotted on a strip-chart recorder. The sample temperature was controlled by a flow of cooled nitrogen gas and measured (±1 K) by using a copper/constantan thermocouple and digital thermometer. The sample-coil supports were Teflon for the ^1H and Lucite for the ^{19}F spin–lattice relaxation time measurements.

The mid- and far-IR spectra were recorded for the samples deposited as thin layers on KBr (mid-IR, Wilmad Co.) and polyethylene (far-IR) windows. Low-temperature FT-IR spectra (ca. 80 K) were obtained by using a Cryodyne Cryocooler (Cryogenics Technology, Inc., Model 21). Raman spectra were measured on an Instruments S.A. Ramanor U-1000 spectrometer for the powdered solids on microscope slides. The spectral measurements were performed under computer control (Columbia Data Products) by using the commercial software supplied by Instruments S.A. The instrument was operated in the micro-Raman configuration in order to minimize sample decomposition in the slightly defocused laser beam (He-Ne model SLR-5P, 5 mW, Optikon Co.), with a 32× long-range microscope objective (180° scattering).

Differential scanning calorimetric measurements were made on a Perkin-Elmer Model 21 calorimeter. Atom–atom potential energy calculations were performed by using programs written in our laboratory for an IBM-PC.

Results and Discussion

X-ray Powder Diffraction Analysis. The molybdenum complex, $[TrMo(CO)_3]BF_4$, crystallizes in the orthorhombic space group *Pbca* (D_{2h}^{15}) with a = 16.297 (2), b = 12.955 (2), and c = 11.749 (2) Å and eight molecules per unit cell.[25] The structures of the chromium and tungsten analogous have not been determined, but it is expected that the three $[TrM(CO)_3]BF_4$ complexes should be isostructural, as has already been found for the related (η^5-C_5H_5)- and (η^6-C_6H_6)$M(CO)_3$ complexes.[8,9,27] Unfortunately, because of their instability in aqueous solution or acetone, even under a nitrogen atmosphere, good quality crystals of the Cr and W salts suitable for X-ray diffraction could not be obtained. However, it was possible to compare the X-ray powder patterns of the three salts.

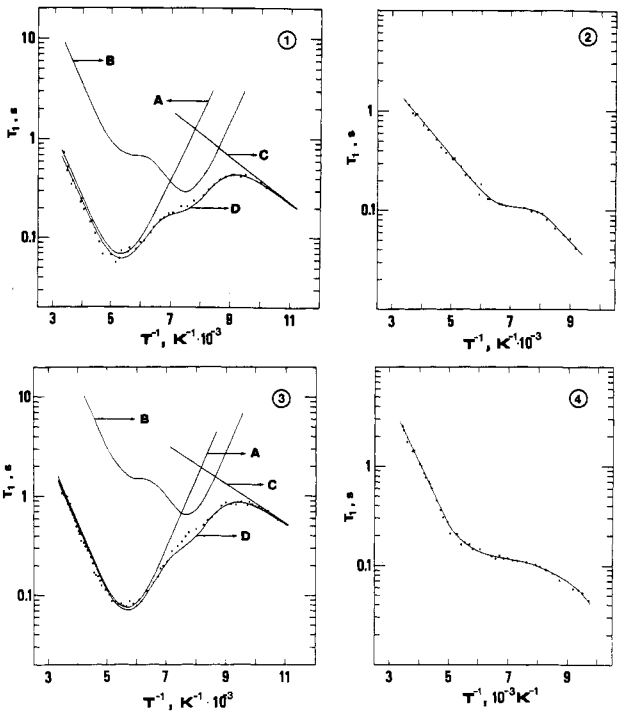

Figure 1. Plots of ^1H (1 and 3) and ^{19}F (2 and 4) spin–lattice relaxation times vs. reciprocal temperature for $[TrCr(CO)_3]BF_4$ (1 and 2) and $[TrMo(CO)_3]BF_4$ (3 and 4), where curves A–C are the best calculated fits for eq 2, 4, and 5, respectively, and curves D are the sums.

The d values, relative intensities (I), and indexations of each diffracted line are given in Table I. A comparison of the d values and their relative intensities shows that they are very similar for all three complexes and, in many cases, identical within experimental error. This provides evidence that the three salts are indeed isostructural. The number of observed diffracted lines increases as Cr < Mo < W, because of the increasing electron density in the unit cells. The best fits between the calculated and observed d values allowed us to obtain the unit cell dimensions for the three complexes. For $[TrMo(CO)_3]BF_4$, our results are in good agreement with the single-crystal unit cell dimensions.[24] The unit cell dimensions from the powder work are also listed in Table I. There is ca. 60 Å^3 increase in unit cell volume between the Cr and Mo complexes and ca. 30 Å^3 between the Mo and W complexes. For these volume changes with changes in metal, the a and c axes are the most affected, while the b axis remains essentially the same.

Spin–Lattice Relaxation Time Measurements. Plots of the experimental T_1 values for both ^1H and ^{19}F nuclei vs. reciprocal temperature are shown in Figure 1 for $[TrM(CO)_3]BF_4$, where M = Cr and Mo. These data cannot be explained by a single relaxation process. The rate of nuclei relaxation is given by a summation over different processes (eq 1). The contribution to

$$\frac{1}{T_1(\text{exptl})} = \sum_i \frac{1}{T_1(i)} \tag{1}$$

the spin–lattice relaxation by homonuclear dipolar coupling in the solid state between nuclei of the same type is given by

$$\frac{1}{T_1} = \frac{2}{3}C_1\left[\frac{\tau}{1+\omega_i^2\tau^2} + \frac{4\tau}{1+4\omega_i^2\tau^2}\right] \tag{2}$$

with

$$\tau = \tau_0 \exp(E_a/RT) \tag{3}$$

where C_1 is a constant related to the change in a second moment

(25) Clark, G. R.; Palenik, G. J. *J. Organomet. Chem.* **1973**, *50*, 185.
(26) King, R. B. *Organometallic Syntheses*; Academic: New York, 1965; Vol. I.
(27) Chhor, K. Ph.D. Thesis, Université de Paris, 1982.
(28) Delisle, P.; Allegra, G.; Mognasecki, E. R.; Chierico, A. *J. Chem. Soc., Faraday Trans. 2* **1975**, 207.

Table I. X-ray Powder Pattern Results for the $[TrM(CO)_3]BF_4$ (M = Cr, Mo, W) Complexes[a]

Cr			Mo			W			*hkl* indexation		
line no.	*I*	*d*, Å	line no.	*I*	*d*, Å	line no.	*I*	*d*, Å			
			1	5	6.997 (8)	1	15	6.958 (8)	210		
1	5	6.559 (8)	2	4	6.511 (8)	2	10	6.511 (8)	020		
2	100	5.848 (8)	3	100	5.965 (8)	3	100	5.945 (8)	211		
3	70	5.651 (8)	4	50	5.669 (8)	4	50	5.687 (8)	021		
4	6	5.356 (7)	5	1	5.379 (7)	5	1	5.395 (7)	121		
5	8	5.059 (7)	6	1	5.096 (7)	6	1	5.088 (7)	112	220	
6	7	4.683 (7)	7	1	4.737 (7)	7	1	4.748 (7)	202		
						8	18	4.575 (7)	311		
7	65	4.418 (6)	8	60	4.466 (6)	9	20	4.468 (6)	212		
8	50	4.322 (6)	9	50	4.339 (6)	10	10	4.332 (6)	022		
9	15	4.017 (6)	10	30	4.062 (6)	11	15	4.077 (6)	400		
10	2	3.936 (6)	11	2	3.934 (6)	12	1	3.943 (6)	321	131	
11	20	3.813 (6)	12	10	3.810 (6)	13	20	3.839 (6)	230	312	
12	15	3.629 (5)	13	4	3.681 (5)	14	25	3.742 (5)	411		
						15	1	3.597 (5)	231		
13	1	3.372 (5)	14	10	3.423 (5)	16	12	3.401 (5)	132	213	
			15	10	3.305 (5)	1	12	3.314 (5)	421		
14	10	3.238 (5)	16	8	3.246 (5)	18	6	3.211 (5)	040	331	
			17	12	3.126 (5)	19	6	3.126 (5)	041		
15	10	2.909 (4)	18	20	2.936 (4)	20	4	2.928 (4)	332	004	
						21	8	2.827 (4)	114		
16	3	2.671 (4)	19	2	2.702 (4)	22	1	2.696 (4)	214		
17	1	2.616 (4)	20	4	2.646 (4)	23	1	2.653 (4)	432	124	
18	5	2.557 (4)	21	15	2.589 (4)	24	8	2.590 (4)	304	611	423
			22	4	2.485 (4)	25	1	2.486 (4)	441		
19	8	2.421 (4)	23	15	2.418 (4)	26	6	2.417 (4)	251		
			24	3	2.877 (4)				532[b]		
						27	1	2.374 (4)	433[b]		
			25	5	2.330 (3)				442		
20	4	2.629 (3)	26	4	2.302 (3)	28	4	2.325 (3)	622		
21	2	2.179 (3)	27	3	2.217 (3)	29	3	2.220 (3)	334		
			28	3	2.149 (3)				514	451	
						30	2	2.130 (3)	061		
			29	3	2.090 (3)	31	2	2.087 (3)	260	253	
			30	1	2.030 (3)	32	1	2.032 (3)	062		
			31	1	1.979 (3)	33	1	1.981 (3)	361		
			32	1	1.918 (3)	34	1	1.924 (3)	552	444	821
			33	1	1.847 (3)	35	1	1.848 (3)[c]			
			34	1	1.809 (3)	36	1	1.811 (3)	270		
						37	1	1.786 (3)	561	271	
						38	1	1.757 (3)	416	454	172

[a] Unit cell parameters: for M = Cr, a = 16.05 (2) Å, b = 12.96 (2) Å, c = 11.64 (2) Å; for M = Mo, a = 16.28 (2) Å, b = 12.97 (2) Å, c = 11.73 (2) Å; for M = W, a = 16.36 (2) Å, b = 12.99 (2) Å, c = 11.79 (2) Å; from ref 25 for M = Mo, a = 16.297 (2) Å, b = 12.955 (2) Å, c = 11.749 (2) Å. [b] Probably the same line. [c] Too many possibilities.

of the resonance line, ω is the resonance frequency of the resonant nucleus, and τ is a correlation time for the motion with E_a as energy of activation. In systems having other spins, the heteronuclear contribution to relaxation is described by eq 4, where ω_2

$$\frac{1}{T_1} = C_2\left[\frac{\tau}{1 + (\omega_1 - \omega_2)^2\tau^2} + \frac{3\tau}{1 + (\omega_1)^2\tau^2} + \frac{6\tau}{1 + (\omega_1 + \omega_2)^2\tau^2}\right] \quad (4)$$

is the precession frequency of the nonresonant nucleus.[29] For homonuclear dipolar interactions only, eq 2 leads to a V-shaped curve having a minimum when $\omega\tau = 0.6158$. It is clear from Figure 1 that this is not true for the whole curve. Minima appear for the $[TrM(CO)_3]BF_4$ complexes in the case of proton spin–lattice relaxation at ca. 0.06 s (187 K) for the Cr complex and ca. 0.07 s (175 K) for the Mo complex. The data were fit by nonlinear least-squares procedures to eq 2 and 4. This, however, did not explain the T_1 values below 110 K, and a third relaxation contribution was added, eq 5, where C_3 and E_a are a preexponential

$$\frac{1}{T_1} = C_3 \exp(E_a/RT) \quad (5)$$

(29) Abragam, A. *The Principles of Nuclear Magnetism*; Oxford University Press: London, 1961.

Table II. Barriers to Rotation for (π-Arene)metal Tricarbonyl Complexes Determined by Proton Spin–Lattice Relaxation Time Measurements

	$10^{-9}C_1$, rad s^{-2}	$10^{-9}C_2$, rad s^{-2}	$10^{13}\tau_0$, s	10^2C_3, s^{-1}	E_a, kJ mol^{-1}	ref
			π-Arene Ring Rotation			
$[TrCr(CO)_3]BF_4$	2.09	0.080	7.85	...	12.8	*b*
				1.24	4.4	
$[TrMo(CO)_3]BF_4$	1.94	0.037	2.64	...	13.6	*b*
				1.16	3.8	
$BzCr(CO)_3$	1.9	...	0.42	...	17.6	28
$CpMn(CO)_3$	2.70	...	6.45	...	7.24	18
$CpRe(CO)_3$	2.25	...	5.43	...	7.15	18
$CbFe(CO)_3$[a]	0.55	...	0.41	...	15.2	16
	0.83	...	0.017	...	22.1	
			BF_4^- Anion Rotation			
$[TrCr(CO)_3]BF_4$	0.0035	0.95	0.62		6.77	*b*
$[TrMo(CO)_3]BF_4$	0.55	1.17	0.13		12.2	*b*

[a] Cb = η^4-C_4H_4. [b] Present work.

constant and a new activation energy, respectively. The solid lines A, B and C in Figure 1 are the best fits for the three equations. Curve D is the summation of the three sets of equations according to eq 1.

In the high-temperature region, curves A and B provide activation energies to ring rotation, and the C_1, C_2, and τ_0 parameters may be deduced from the best calculated fits. Curve A represents

essentially ^1H–^1H dipolar interactions, while curve B describes the ^1H–^{19}F dipolar interactions. It is important to notice that curve B possesses a minimum and an inflection point. No better fits were obtained in considering nuclei such as ^{10}B and ^{11}B in the proton relaxation. The results are presented in Table II. The barriers to Tr ring rotation for the Cr and Mo complexes are 12.8 and 13.6 kJ mol^{-1}, respectively. The close proximity of the two values is not too surprising since these complexes are isostructural with similar packing densities. The activation energies for ring rotation in various π-arene metal tricarbonyl complexes are compared in Table II. There is no obvious correlation between arene ring size and activation energy. The latter must depend on the crystal packing and intermolecular forces involved.

The third proton relaxation process gave as a preexponential factor, C_3, values of 1.24×10^{-2} and 1.16×10^{-2} s^{-1} with activation energies of 4.4 and 3.8 kJ mol^{-1} for the Cr and Mo complexes, respectively. These processes are only efficient in the low-temperature range. Such activation energies are rather low, and we are unable to account for this relaxation process with any confidence. The presence of paramagnetic impurities causing relaxation at low temperature is a possibility. The ^{19}F spin–lattice relaxation time measurements as a function of temperature are also given in Figure 1. Inflection points are observed as ca. 0.11 s (141 K) for the Cr complex and at ca. 0.12 s (149 K) for the Mo complex.

The ^{19}F spin–lattice relaxation times were very difficult to fit because it is clear that an intermolecular heteroatomic spin exchange is responsible for fluorine relaxation. Although the boron atoms are closer to the fluorines than are the hydrogens to the fluorines, the large differences in precession frequencies between ^{10}B and ^{11}B with ^{19}F and ^1H makes these interactions much less insignificant (eq 4). Nevertheless, for $\omega_1 = \omega_F$ and $\omega_2 = \omega_H$, acceptable fits are obtained with activation energies for BF_4^- reorientation of 6.77 and 12.2 kJ mol^{-1} for the Cr and Mo complexes, respectively. These detailed results are also presented in Table II. For the Cr complex, such an activation energy is readily explained by the high degree of reorientation of the BF_4^- anion. On the other hand, 12.2 kJ mol^{-1} for the Mo complex is really quite large for such motions. It is possible that the contributions to ^{19}F–^{10}B and ^{19}F–^{11}B interactions are different for both complexes.

For π-arene ring rotation, the internal barrier to rotation is essentially zero.[1,2] The barriers in the solid state arise from intermolecular sources; i.e., they are dependent on crystal packing. On the other hand, the X-ray results of the BF_4^- ion in the Mo complex show clear evidence of disorder due to dynamic effects. On the basis of the crystal data known for the Mo complex, it should be possible to confirm our NMR results by atom–atom potential calculations and to so identify the different contributions to the barriers to molecular and ring reorientation. These calculations will be the subject of the next section.

Atom–Atom Potential Calculations. The individual energies of interatomic interactions between molecules (or atoms) in a solid are assumed to be additive, and each term depends only on the interatomic distances. By the use of a method described elsewhere,[18] the atomic positions are input into the computer program and an arbitrary 8-Å cutoff is used in order to save computer time. The Buckingham expression given in eq 6 was used, where A, B,

$$V(r) = Ar^{-6} + B\exp(-Cr) \quad (6)$$

and C are parameters characteristic of a given atom pair. These parameters are derived by fitting experimental data such as molecular or crystal structures, heats of sublimation, lattice energies, elastic constants, etc. For heteroatomic interactions, the combining rules shown in eq 7, were applied. The parameters

$$A_{ij} = (A_{ii}A_{jj})^{1/2} \quad (7a)$$

$$B_{ij} = (B_{ii}B_{jj})^{1/2} \quad (7b)$$

$$C_{ij} = (C_{ii} + C_{jj})/2 \quad (7c)$$

suggested by Mirsky[30] were used for C–C, H–H, and O–O interactions. For the B–B and F–F parameters, the empirical eq 8, proposed by Gavezotti and Simonetta,[31] was used, where d_0

$$V(r) = 3000\exp(-13r/d_0) - 0.14(d_0/r)^6 \quad (8)$$

is the sum of the van der Waals radii (in Å) of the two atoms involved in the potential; the d_0 values were taken from ref 32. The list of the nonbonded atom–atom potential function constants is given in Table III. Interactions involving the metal atoms have little effect on the calculated barrier height,[18] and therefore these contributions were omitted from the calculations.

Table III. Nonbonded Atom–Atom Potential Function Constants[a]

atoms	A, kJ mol^{-1}	$10^{-4}B$, kJ mol^{-1}	C, Å^{-1}
C–C	1761	29.96	3.68
H–H	121	2.05	4.29
O–O	1085	32.51	4.18
F–C	629	1.26	4.06
F–H	161	1.26	5.10

[a] From eq 8 written in the form $V(r) = -Ar^{-6} + B\exp(-Cr)$.

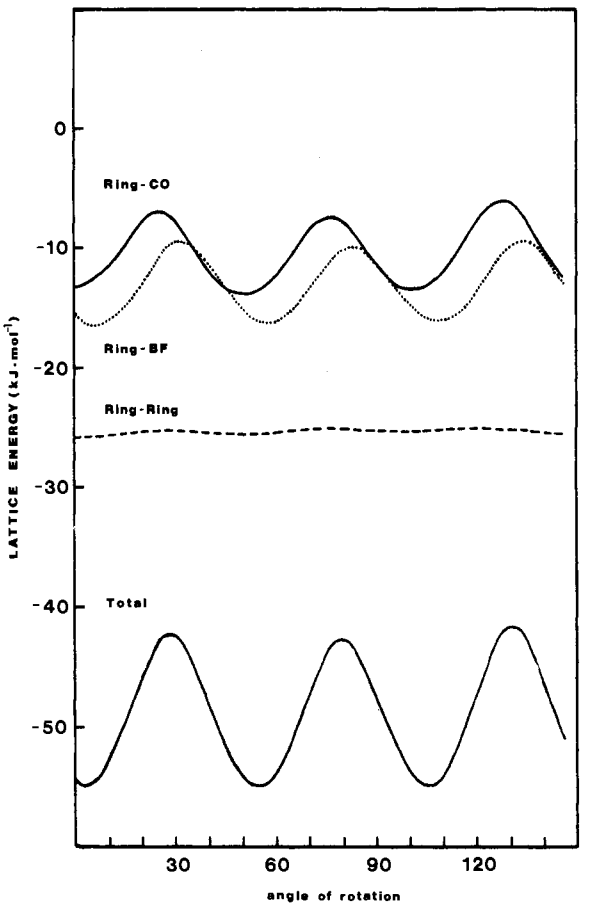

Figure 2. Variation of potential energy calculated for $[TrMo(CO)_3]BF_4$ with change in angle of Tr ring rotation.

The potential energy calculations were performed for different angles of rotation of the arene ring around the molecular axis and, in the case of the BF_4^- ion, along the four C_3 axes and the six C_2 axes of a "probe" molecule in a rigid lattice.

Figure 2 shows the variation of the calculated potential energy environment of $[TrMo(CO)_3]BF_4$ as a function of the angle of Tr ring rotation. The calculated barrier height, taken from the difference between the minimum and maximum values of the total

(30) Mirsky, K. *Computing in Crystallography*; Delft University Press: Delft, The Netherlands, 1978.
(31) Gavezotti, A.; Simonetta, M. *Acta Crystallogr., Sect. A: Cryst. Phys. Diffr., Theor. Gen. Chem.* **1975**, *31*, 645.
(32) Pauling, L. *The Nature of the Chemical Bond*, 2nd ed.; Cornell University Press: Ithaca, NY, 1948.

Table IV. Vibrational Numbering for $[TrM(CO)_3]BF_4$[a]

	(a) C_7H_7 Vibrations (C_{7v} Symmetry)				
a_1	CH str	ν_1	e_2	CH str	ν_{12}
	CC str	ν_2		CC str	ν_{13}
	CH oop def	ν_3		CH cp def	ν_{14}
	M–ring str	ν_4		CH oop def	ν_{15}
				CCC cp def	ν_{16}
				CCC oop def	ν_{17}
a_2	CH ip def	ν_5			
	$(CO)_3$M-ring torsion	ν_6			
e_1	CH str	ν_7	e_3	CH str	ν_{18}
	CC str	ν_8		CC str	ν_{19}
	CH ip def	ν_9		CH ip def	ν_{20}
	CH oop def	ν_{10}		CH oop def	ν_{21}
	Mring tile	ν_{11}		CCC cp def	ν_{22}
				CCC oop def	ν_{23}
	(b) $M(CO)_3$ Vibrations (C_{3v} Symmetry)				
a_1	CO str	ν_{24}	e	CO str	ν_{29}
	MCO def	ν_{25}		MCO def	ν_{30}
	MC str	ν_{26}		MCO def	ν_{31}
	CMF def	ν_{27}		MC str	ν_{32}
				CMC def	ν_{33}
a_2	MCO def	ν_{28}		ring–$M(CO)_3$ def	ν_{34}
	(c) BF_4 Vibrations (T_d Symmetry)				
a_1	BF str	ν_{35}	t_1	FBF def	ν_{37}
e	F_2BF_2 torsion	ν_{36}	t_2	BF str	ν_{38}

[a] Key: ip, in plane; oop, out of plane.

barrier, is 12.6 kJ mol^{-1}, which is in good agreement with the NMR results. The different contributions to the barrier are also shown in Figure 2, where it can be seen that the major terms arise from ring–BF and ring–CO interactions. The latter are almost exclusively intermolecular in origin, since the internal barrier is very small. The ring–ring interactions only make a minor contribution, and, therefore, cooperative motions involving the rings are unlikely. Ring–BF_4 interactions, on the other hand, may well be cooperative.

The barrier calculations for the BF_4^- ions are more complicated because the atomic positions in the Mo complex are (apparently) incorrect and the B–F distances exhibit large variations. For two sets of data, real atomic positions, and ideal tetrahedral geometry (with equal B–F bond distances), the calculations of the potential energies as a function of C_2 and C_3 rotation lead to asymmetric barriers in the C_2 case and symmetric ones for C_3. But the most important observation is the barrier to C_3 rotation is smaller than that for C_2 rotation. Moreover, there seems to be some dependences of the barrier on which particular C_3 (or C_2) axis is chosen; the values fall in the 8–16 kJ mol^{-1} range. The average barrier height (ca. 12 kJ mol^{-1}) is in the same range as the activation energy for BF_4^- ion reorientation measured by the NMR method (12.2 kJ mol^{-1}). This provides further support for attributing the ^{19}F lattice relaxation to rotation about the 3-fold axes.

Vibrational Spectra. Although the vibrational spectra of the planar (D_{7h} symmetry) tropylium cation, $C_7H_7^+$, have been thoroughly investigated and assignments proposed for the various modes,[33-38] the spectra of complexes containing the $(\eta^7\text{-}C_7H_7)^+$ ligand have received relatively little attention. In the case of the $[TrM(CO)_3]BF_4$ (M = Cr, Mo, W) and $TrV(CO)_3$ complexes, IR data for the CO stretching modes and Raman and far-IR results for vibrations below 1000 cm^{-1} have been reported,[39-41]

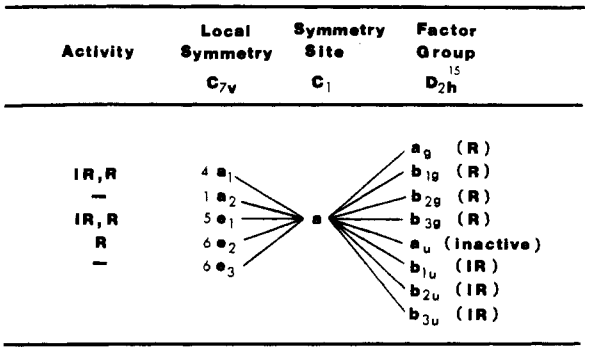

Figure 3. Correlation diagram for solid $[TrM(CO)_3]BF_4$.

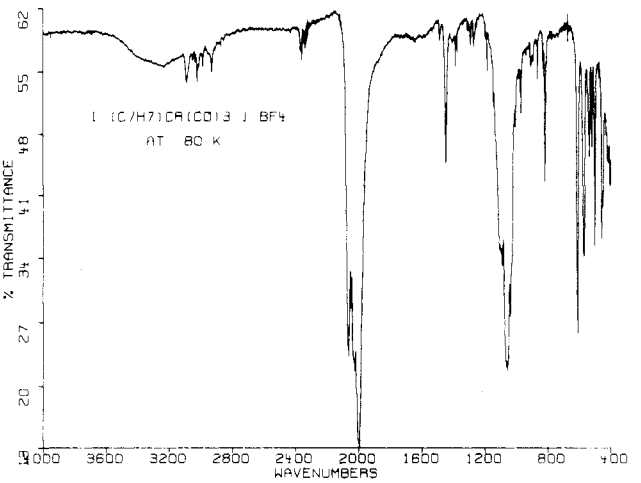

Figure 4. FT-IR spectrum of solid $[TrCr(CO)_3]BF_4$ deposited on a KBr window at 80 K (800 scans, 1-cm^{-1} resolution).

while a few vibrational assignments have been published for the metallocene TrMCp (M = Ti, V; Cp = η^5-C_5H_5).[42,43]

The vibrational spectra of (π-arene)metal tricarbonyl complexes are customarily analyzed in terms of the local symmetries of the (π-arene)M and $M(CO)_3$ fragments. The 39 vibrational modes of the $(\eta^7\text{-}C_7H_7)M$ moiety in $[TrM(CO)_3]BF_4$, assuming C_{7v} local symmetry, span the following representations: $4a_1$ (IR/R) + a_2 (inactive) + $5e_1$ (IR/R) + $6e_2$ (R) + $6e_3$ (inactive). The C_{3v} $M(CO)_3$ moiety has 15 modes: $4a_1$ (IR/R) + a_2 (inactive) + 5e (IR/R). Three additional modes involve both moieties and are treated separately: ring rotation or torsion (a_2; C_{7v}) and ring–M–$(CO)_3$ deformation (e; C_{3v}). However, the torsional mode has a frequency of zero due to an absence of an internal barrier of rotation. Finally, the BF_4^- ion (T_d symmetry) has nine vibrational modes distributed as a_1 (R) + e (R) + t_1 (inactive) + t_2 (IR/R). Table IV gives the numbering and description of each normal mode.

Because of the low site symmetry (C_1) of the crystalline $[TrM(CO)_3]BF_4$ complexes, each mode is both IR and Raman active (Figure 3). With eight molecules per unit cell and D_{2h}^{15} as the factor group, the correlation diagram predicts 9, 6, or 3 bands in the IR spectra of the solid complexes for each triply

(33) Kitaigorodskii, A. I.; Struchkov, Y. T.; Khotsyama, T. L.; Vol'pin, M. E.; Kursanov, D. N. *Izv. Akad. Nauk SSSR, Ser. Khim.* **1960**, *1*, 39.
(34) Garbuzova, I. A.; Kolomvikova, G. D.; Aleksanyan, V. T. *Izv. Akad. Nauk SSSR, Ser. Khim.* **1983**, 112.
(35) Sourisseau, C. *Spectrochim. Acta, Part A* **1978**, *33A*, 881.
(36) Fateley, W. G.; Curnutte, B.; Lippincott, E. R. *J. Chem. Phys.* **1957**, *26*, 1471.
(37) Nelson, R. D.; Fateley, W. G.; Lippincott, E. R. *J. Am. Chem. Soc.* **1956**, *78*, 4870.
(38) Fateley, W. G.; Lippincott, E. R. *J. Am. Chem. Soc.* **1955**, *77*, 249.
(39) Abel, E. W.; Bennett, M. A.; Burton, R.; Wilkinson, G. *J. Chem. Soc.* **1958**, 455.
(40) Fischer, R. D. *Z. Naturforsch., A: Astrophys., Phys., Phys. Chem.* **1963**, *18A*, 1373.
(41) Howard, J.; Graham, D. *Spectrochim. Acta, Part A* **1985**, *41A*, 815.
(42) van Oven, H. O.; de Liefde Meyer, H. J. *J. Organomet. Chem.* **1970**, *23*, 13.
(43) King, R. B.; Stone, F. G. A. *J. Am. Chem. Soc.* **1959**, *81*, 5263.
(44) Adams, D. M.; Squire, A. *J. Organomet. Chem.* **1973**, *63*, 381.
(45) Fritz, H. P.; Manchot, J. *Spectrochim. Acta* **1962**, *18*, 171.
(46) The periodic group notation in parentheses is in accord with recent actions by IUPAC and ACS nomenclature committees. A and B notation is eliminated because of wide confusion. Groups IA and IIA become groups 1 and 2. The d-transition elements comprise groups 3 through 12, and the p-block elements comprise groups 13 through 18. (Note that the former Roman number designation is preserved in the last digit of the new numbering: e.g., III → 3 and 13).

Table V. List of Vibrational Frequencies (±1 cm^{-1}) for Solid $[(\eta^7\text{-}C_7H_7)M(CO)_3]BF_4$ at 80 K and Room Temperature (M = Cr and Mo)

M = Cr		M = Mo			M = Cr		M = Mo		
FTIR 80 K	FTIR 300 K	FTIR 300 K	Raman	assignt[b]	FTIR 80 K	FTIR 300 K	FTIR 300 K	Raman	assignt[b]
3089 w sh				CH str (e_3), ν_{18}	1108 s	1103 s	1100 s		BF str (a_1), ν_{35}
3084 w	3085 w	3081 w			1099 s	1092 s	1090 s		
3077 w	3079 w sh	3069 w sh		CH str (a_1), ν_1	1090 s				
3055 vw				CH str (e_2), ν_{12}	1072 vs sh				BF str (t_2), ν_{38}
3047 vw	3048 vw				1065 vs				
3037 vw	3033 vw	3029 vw sh			1058 vs				
3018 w	3022 w sh			CH str (e_1), ν_7	1051 vs	1058 vs br	1057 vs br		
3011 w	3011 w	3012 vw			1040 vs	1040 vs	1039 vs		
2982 w	2985 w				1027 vs	1026 s sh			
2967 vw sh	2955 vw sh	2956 vw sh		combinations and overtones	1013 m	1011 m sh	1004 m		CH oop (e_2), ν_{15}
2947 vw					1004 m	1003 m	997 m		
2932 w	2928 vw	2827 vw			983 w				CH ip def (e_1), ν_9
2906 vw	2906 vw sh				979 w	979 m	969 m		
2881 vw	2978 vw	2975 vw			973 m	973 m	963 m		
2870 vw	2852 vw				969 m	969 m	959 m		
2845 vw					910 w				
2070 vs sh				CO str (a_1), ν_{24}	906 w	908 w sh			CH oop def (e_1), ν_{10}
2065 vs	2064 vs	2089 vs			902 w	902 w	903 w		
2050 s	2050 s sh				896 w	896 w	896 w		
2037 vs sh	2039 s sh	2045 s sh	2046 m w	CO str (e), ν_{29}; combinations and overtones	893 w	892 w	891 w		
2033 vs sh					863 w	864 w	861 w		
2026 vs	2025 vs	2029 vs	2027 m		861 w	861 w sh	858 w sh		CC str (a_1), ν_2
2016 vs sh	2018 vs	2018 vs sh			857 w				
1005 vs	2004 vs	2006 vs sh			830 w	829 w			
2002 vs		2002 vs	2002 m		826 w	824 w			
1996 vs	1994 s sh				817 m	816 m	816 m sh		CCC ip def (e_3), ν_{22}
1989 vs sh					814 m	812 ms	808 ms		
1977 s sh	1978 m sh	1976 m sh			806 w	807 w sh	805 sh		
1968 mw	1970 w sh			^{13}CO str	786 vw				
1960 mw					779 vw	772 vw	774 vw		CCC oop def (e_3), ν_{23}
1958 mw	1959 w				773 vw	770 vw sh	770 vw		
1486 w					767 vw	767 vw			
1482 w	1483 w	1476 w		CC str (e_2), ν_{13}	614 s				CH oop def (a_1), ν_3
1476 w sh		1468 w			610 s	605 s	604 m		
1453 m		1457 w sh			582 m sh				
1447 m		1451 w sh		CC str (e_1), ν_8	576 m	569 m sh	563 m		MCO def (e), ν_{30}
1445 m sh	1448 m	1440 m			569 m	565 m	558 ms		
1440 m		1431 m sh			549 ms	541 m sh	533 w		
1385 w		1384 vw			543 m				MCO def (e), ν_{31}
1382 w sh	1378 w	1370 vw		CH cp def (a_2), ν_5	537 m				
1373 w	*a*	1354 vw			534 m	535 m	523	m	
1335 vw	1335 vw	1335 vw			521 m	522 m	514	m	MCO def (a_1), ν_{25}
1312 w sh					502 m				
1307 w					499 m sh	499 m	499 m		FBF def (t_1), ν_{37}
1300 w	1300 w sh			CC str (e_3), ν_{19}			480 m	485 vw	M(CO) str (e), ν_{32}
1296 w					477 w		475 m sh		
1293 w					459 m	454 m sh	459 w sh		CCC cp def (e_2), ν_{16}
1288 w	1288 w	1285 w			451 m	445 m	445 w		
1277 vw						421 w sh			M(CO) str (a_1), ν_{26}
1271 w sh						415 m	405 m	405 vw	
1266 w	1267 w	1260 w		CH ip def (e_2), ν_{14}		352 vw	353 vw		CCC oop def (e_2), ν_{17}
1262 w	1264 w sh	1257 w sh				323 w	334 w	331 m	ring M tilt (e_1), ν_{11}
1257 w sh						315 w	324 w	324 m	
1249 w						303 w	308 m	309 vs	
1193 w	1191 vw			CH ip def (e_3), ν_{20}				302 m sh	ring M str (a_1), ν_4
1187 w							296 w sh	295 w sh	
1184 w								100 s v br	CMC def (a_1 + e), ν_{33}, ν_{27}
1182 w sh	1181 vw								
1144 w	1142 w sh			CH oop def (e_3), ν_{21}				22 m sh	lattice
1131 w sh									

[a] Multicomponent. [b] Key: ip, in plane; oop, out of plane.

degenerate (BF_4^- vibrations), doubly degenerate, and nondegenerate mode, respectively. At room temperature, the IR bands are broad and the necessary resolution must be achieved by a low-temperature study, especially for $[TrCr(CO)_3]BF_4$ (Figure 4). The observed vibrational frequencies of the Cr and Mo derivatives are listed in Table V. Unfortunately, no Raman data using 488.0-, 514.5-, 588.0-, or 632.8-nm excitation could be obtained for the Cr complex due to its particularly high thermal sensitivity and dark orange color, even when a spinning cell or cryogenic and microscopic techniques are used with the different laser lines. The light orange Mo complex was somewhat better when the 632.8-nm excitation line of a He–He laser was used, but only selected Raman bands could be detected (Figure 5). These bands are assigned to Mo–C stretches, Mo–ring stretch and tilts, CMoC and ring–$Mo(CO)_3$ deformations, and, finally, CO stretches. It is clear that vibrations of the "isolated" tropylium ligand and tetrafluoroborate anion are missing or too weak to be observed. This situation is most probably a consequence of resonance Raman effects, but we could not verify this since irradiation with higher laser frequencies resulted in sample decomposition.

A comparison of the vibrational frequencies reported for various tropylium salts in the literature[38-43] reveals that there are no drastic

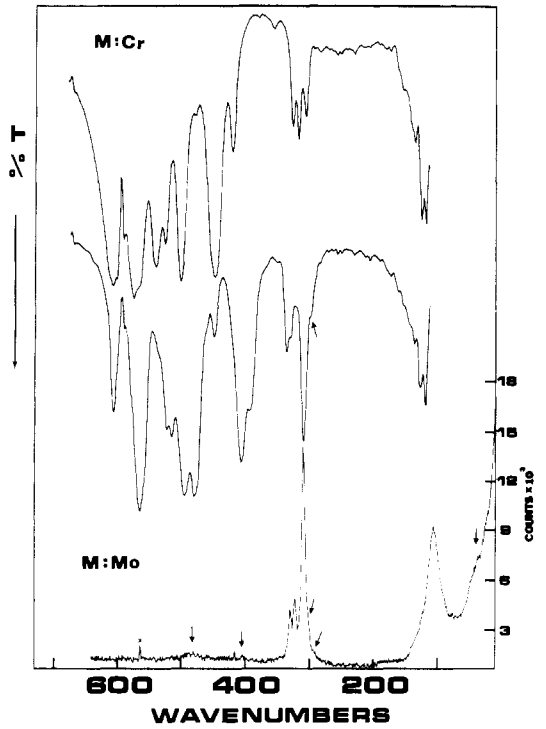

Figure 5. Far-IR spectra of $[TrM(CO)_3]BF_4$ (M = Cr, Mo) at room temperature (300 scans, 2-cm^{-1} resolution). Micro-Raman spectrum of $[TrMo(CO)_3]BF_4$ at room temperature (632.8-nm excitation, 2.5 mW at sample; 300-μm slits; 32 scans at 2 s $point^{-1}$ spaced by 1 cm^{-1}; 32× long-range objective; no smoothing or base line correction; × = noise spike).

Table VI. Comparison of the Vibrational Frequencies (cm^{-1}) of Free and Complexed Tropylium Ligand in $[TrM(CO)_3]BF_4$ (M = Cr, Mo)

$C_7H_7^+$ (D_{7h})[a]	(η^7-C_7H_7)Cr[b]	(η^7-C_7H_7)Mo[b]	assignt[d]	
3020	3017	3012	CH str	(e_1)
3072	3079	3069	CH str	(a_1)
3085	3085	3081	CH str	(e_3)
3042	3041	3029	CH str	(e_2)
1596	1483	1472	CC str	(e_2)
1477	1448	1448	CC str	(e_1)
1309	1378	1369	CC cp def	(a_2)
1282	1294	1285	CC str	(e_3)
1224	1266	1269	CH ip def	(e_2)
1100	1186	*c*	CH ip def	(e_3)
1025	1142	*c*	CH oop def	(e_3)
1025	1007	1001	CH oop def	(e_2)
993	974	964	CH ip def	(e_1)
892	900	897	CH oop def	(e_1)
869	863	861	CC str	(a_1)
768	818	810	CCC ip def	(e_3)
648	770	772	CCC oop def	(e_3)
648	605	604	CCC oop def	(a_1)
430	450	452	CCC ip def	(e_2)
353	352	353	CCC oop def	(e_3)

[a] Reference 39. [b] Average value taken from Table V. [c] Not observed. [d] Key: ip, in plane; oop, out of plane.

changes in the tropylium vibrational frequencies on changes in the anion. Large changes are observed when the ligand is complexed to a metal however. The comparison of free and complexed tropylium vibrational frequencies is given in Table VI. The C–H stretching frequencies remain similar, but two of the CC stretches of the free ligand shift from 1596 and 1477 to 1483 and 1448 cm^{-1}, respectively, while two others remain essentially constant—1282 and 869 cm^{-1} compared to 1290 and 862 cm^{-1}. We failed to detect any weak band between 1500 and 1650 cm^{-1}, even at 80 K. While two CC stretching vibrations decrease in energy, the CH in-plane deformation vibrations increase with one exception: 1309, 1225, 1100, and 993 cm^{-1} to 1374, 1268, 1186, and 969 cm^{-1}, respectively. This is also true for the in-plane skeletal deformations: 768 and 430 cm^{-1} to 814, and 451 cm^{-1}, respectively. Concerning out-of-plane modes, these shift in both directions but mainly show a slight decrease in energy. The tropylium modes (as well as the BF_4^- vibrations) exhibit little temperature dependence. When the central metal is changed from Cr to Mo, there is a small decrease in the tropylium vibrational frequencies suggesting a somewhat higher electronic density in the ring system of the Cr complex. The large decreases in frequency for the CC stretches (e_1 and e_2) between the free and complexed tropylium demonstrate the transferral of electron density from the Tr ligand to the metal on complex formation.

Table VII. Comparison of a Few Important Vibrations (cm^{-1}) of Solid (η^n-C_nH_n)$M(CO)_3$ Complexes

$CbFe^{II}{}_3$[a] (50 K)	$CpMn^0$[b] (175 K)	$BzCr^0$[c] (80 K)	$TrCr^I$[d] (80 K)	assignt	
3150	3120	3100	3086	CH str	
3170	3105	3085	3077		
3103	3095	3075	3045		
		3060	3015		
2036	2015	1980	2062	CO str	a_1
1943	1927	1908	2020		e
1325	1424	1518	1481	CC str	
1310	1363	1448	1446		
		1318	1300		
1235	1113	979	860	ring breath	

[a] Taken from an average in ref 16. [b] Taken from an average in ref 43. [c] Taken from an average in ref 27 and 44. [d] Taken from an average in Table V.

Some selected vibrations of (π-arene)$M(CO)_3$ complexes are compared in Table VII. When arene ring size is changed from 4- to 6-membered, there is a decrease in the CO stretching frequencies, presumably reflecting the decrease in oxidation state from Fe(II) to Cr(0) and the concomitant increase in M–CO π-back-bonding. The CO stretching frequencies increase sharply upon coordination of the $C_7H_7^+$ ring due to the removal of electron density from the metal to the tropylium ligand. The CC ring-breathing mode decreases dramatically from 1235 cm^{-1} for η^4-C_4H_4 in $CbFe(CO)_3$ to 860 cm^{-1} for η^7-$C_7H_7^+$ in $[TrCr(CO)_3]^+$, as a result of the decrease in the associated force constant from the highly strained 4-membered ring to the much more flexible 7-membered one. When the temperature is gradually decreased, the IR spectrum of solid $[TrCr(CO)_3]BF_4$ improves in resolution. No phase transition was observed throughout the temperature range 296–80 K investigated, and this was supported by DSC measurements.

Inelastic neutron-scattering studies[41] of the lattice mode region have lead to the assignment of peaks at 75 cm^{-1} to the ring torsion mode in the Cr and Mo complexes. This value affords a calculated barrier for arene group rotation of about 22 kJ mol^{-1}, which is not in agreement with the NMR results. Such discrepancies have been noted previously for other π-arene ring systems.[16,21]

Acknowledgment. Professor A. L. Beauchamp, M.-J. Olivier, and especially M. Simard (Université de Montréal) are thanked for their warm hospitality and assistance during the X-ray powder diffraction measurements. This research was generously supported by operating and equipment grants from the NSERC (Canada) and the FCAR (Quebec) and graduate scholarships to P.D.H. from the NSERC and McGill University (McConnell and Stewart Foundations).